Available online at www.sciencedirect.com
SCIENCE DIRECT®
Journal of Solid State Chemistry 177 (2004) 2600–2609
JOURNAL OF SOLID STATE CHEMISTRY
http://elsevier.com/locate/jssc

Preparation and crystal structure of ternary rare-earth platinum metal aluminides $R_2T_3Al_9$ (T = Rh, Ir, Pd) with $Y_2Co_3Ga_9$-type structure and magnetic properties of the iridium compounds

Jens Niermann, Birgit Fehrmann, Michael W. Wolff, and Wolfgang Jeitschko*

Institut für Anorganische und Analytische Chemie, Universität Münster, Wilhelm-Klemm-Straße 8, D-48149 Münster, Germany

Received 13 November 2003; received in revised form 27 February 2004; accepted 7 March 2004

Abstract

The ternary aluminides $R_2Rh_3Al_9$ (R = Y, La–Nd, Sm, Gd–Tm, Lu), $R_2Ir_3Al_9$ (R = Y, La–Nd, Sm, Gd–Lu), and $R_2Pd_3Al_9$ (R = Y, Gd–Tm) have been prepared by arc melting of the elemental components with an excess of aluminum and dissolving the aluminum-rich matrix in hydrochloric acid. They crystallize with $Y_2Co_3Ga_9$-type structure: $Cmcm$, $Z = 4$. The crystal structures of $Ho_2Rh_3Al_9$ and $Er_2Ir_3Al_9$ have been refined from single-crystal X-ray data; $Ho_2Rh_3Al_9$: $a = 1316.8(3)$ pm, $b = 760.2(2)$ pm, $c = 933.7(2)$ pm, $R = 0.044$ for 255 structure factors and 27 variables; $Er_2Ir_3Al_9$: $a = 1313.8(2)$ pm, $b = 758.5(1)$ pm, $c = 933.8(2)$ pm, $R = 0.057$ (392 F values, 27 variables). The structure may be viewed as consisting of atomic layers of the compositions $A = R_2Al_3$ and $B = T_3Al_6$ which alternate in the sequence $ABAB$ along the z direction. Approximately 33% and 27% of the A layers were found to be misplaced in the crystals investigated for $Ho_2Rh_3Al_9$ and $Er_2Ir_3Al_9$, respectively. The magnetic properties of most iridium-containing compounds have been determined with a superconducting quantum interference device magnetometer. The yttrium and the lanthanum compounds show Pauli paramagnetism, others reflect the magnetic behavior of the rare-earth components. The magnetic ordering temperatures are all lower than 20 K.

Keywords: Rare-earth compounds; Platinum metals; Aluminides; Crystal structure; Stacking variants; Magnetic properties

1. Introduction

In recent years we have synthesized a large number of ternary rare-earth (R) transition metal (T) aluminides using an excess of aluminum as a flux. Frequently, single-phase materials are obtained after the flux has been dissolved in hydrochloric acid or in aqueous solutions of sodium hydroxide. With the platinum metals as transition metal components, we have already reported on the series of compounds RT_2Al_{10} (T = Ru, Os) [1], the series $R_4T_9Al_{24}$ (T = Pd, Pt) [2], $R_3T_4Al_{12}$ (T = Ru, Os) [3], $R_2Pt_6Al_{15}$ [4], $R_{7+x}Os_{12}Al_{61+y}$ [5], and on the compound $NdRh_4Al_{15.37}$ [6]. We now have included rhodium and iridium as transition metal components and we report here on three series of rare-earth compounds $R_2T_3Al_9$ (T = Rh, Ir, Pd) crystallizing with a structure which has first been established for $Y_2Co_3Ga_9$ [7]. Other aluminides with this structure type, including several compounds with rhodium and iridium, have been synthesized by other research groups: $Y_2Co_3Al_9$ [8], $Gd_2Ir_3Al_9$ [9], $A_2Rh_3Al_9$ (A = La, Ce, U) [10–12], $A_2Ir_3Al_9$ (A = Ce, U) [10–12], and $Yb_2T_3Al_9$ (T = Rh, Ir) [12,13]. Most of these compounds were synthesized in order to investigate their physical properties. Such compounds, especially those containing rare-earth elements, may occur in aluminum alloys as undesired impurities. However, they may also improve their mechanical properties [14–16]. Some results reported here have briefly been presented at a conference [17].

2. Sample preparation and lattice constants

Starting materials were the elemental components, all with nominal purities >99.9%. Aluminum and the platinum metals were used in the form of powders, the

*Corresponding author. Fax: +49-251-8333-136.
E-mail address: jeitsch@uni-muenster.de (W. Jeitschko).

0022-4596/$ - see front matter © 2004 Elsevier Inc. All rights reserved.
doi:10.1016/j.jssc.2004.03.007

Table 1
Lattice constants of ternary aluminides with $Y_2Co_3Ga_9$-type structure[a]

Compound	a (pm)	b (pm)	c (pm)	V (nm^3)	Reference
$Y_2Rh_3Al_9$	1308.2(2)	755.4(1)	942.7(1)	0.9315	This work
$La_2Rh_3Al_9$	1339.3(1)	773.2(1)	954.0(1)	0.9879	This work
$La_2Rh_3Al_9$	1317	773	967	0.984	[10]
$Ce_2Rh_3Al_9$	1330.9(2)	768.3(1)	948.8(1)	0.9702	This work
$Ce_2Rh_3Al_9$	1314.5(5)	768.8(3)	955.9(4)	0.9659	[10]
$Pr_2Rh_3Al_9$	1336.5(2)	771.6(1)	946.1(1)	0.9757	This work
$Nd_2Rh_3Al_9$	1331.8(2)	768.9(1)	949.2(1)	0.9720	This work
$Sm_2Rh_3Al_9$	1331.1(1)	768.5(1)	939.9(1)	0.9615	This work
$Gd_2Rh_3Al_9$	1327.4(1)	766.4(1)	939.0(1)	0.9552	This work
$Tb_2Rh_3Al_9$	1324.1(2)	764.4(1)	936.9(1)	0.9482	This work
$Dy_2Rh_3Al_9$	1322.0(2)	763.2(1)	935.1(1)	0.9435	This work
$Ho_2Rh_3Al_9$	1318.4(2)	761.1(1)	934.7(1)	0.9380	This work
$Er_2Rh_3Al_9$	1315.7(2)	759.6(1)	933.6(1)	0.9331	This work
$Tm_2Rh_3Al_9$	1312.0(2)	757.5(1)	933.8(1)	0.9280	This work
$Yb_2Rh_3Al_9$	1290.6	754.2	938.1	0.9131	[13]
$Lu_2Rh_3Al_9$	1304.4(1)	753.2(1)	936.1(1)	0.9197	This work
$U_2Rh_3Al_9$	1305	761	938	0.932	[10]
$Y_2Ir_3Al_9$	1311.0(2)	750.7(1)	942.2(2)	0.9272	This work
$La_2Ir_3Al_9$	1332.7(1)	769.4(1)	954.0(1)	0.9783	This work
$Ce_2Ir_3Al_9$	1324.3(1)	764.6(1)	947.9(1)	0.9598	This work
$Ce_2Ir_3Al_9$	1305	759	953	0.944	[10]
$Pr_2Ir_3Al_9$	1329.2(2)	767.4(1)	946.3(1)	0.9653	This work
$Nd_2Ir_3Al_9$	1327.0(2)	766.1(1)	945.0(1)	0.9607	This work
$Sm_2Ir_3Al_9$	1326.1(1)	765.6(1)	938.5(1)	0.9529	This work
$Gd_2Ir_3Al_9$	1321.3(3)	763.1(2)	938.8(2)	0.9467	This work
$Gd_2Ir_3Al_9^*$	1326.9(5)	766.0(2)	936.4(2)	0.9518	This work
$Gd_2Ir_3Al_9$	1300.7(2)	759.3(1)	946.6(2)	0.9349	[9]
$Tb_2Ir_3Al_9$	1315.2(2)	756.3(1)	941.4(1)	0.9401	This work
$Tb_2Ir_3Al_9^*$	1317.0(4)	760.3(2)	938.5(2)	0.9398	This work
$Dy_2Ir_3Al_9$	1313.7(2)	753.2(2)	941.0(2)	0.9311	This work
$Dy_2Ir_3Al_9^*$	1313.9(8)	756.0(4)	938.2(3)	0.9318	This work
$Ho_2Ir_3Al_9$	1313.5(2)	752.5(1)	939.7(1)	0.9287	This work
$Ho_2Ir_3Al_9^*$	1314.2(2)	755.6(4)	935.8(2)	0.9293	This work
$Er_2Ir_3Al_9$	1309.4(2)	751.1(1)	938.9(2)	0.9233	This work
$Er_2Ir_3Al_9^*$	1312.7(5)	753.2(3)	938.0(4)	0.9274	This work
$Tm_2Ir_3Al_9$	1308.6(3)	749.0(2)	936.3(2)	0.9177	This work
$Tm_2Ir_3Al_9^*$	1308.9(6)	749.3(3)	935.3(3)	0.9173	This work
$Yb_2Ir_3Al_9$	1305.6(2)	753.7(1)	935.7(2)	0.9208	This work
$Yb_2Ir_3Al_9^*$	1311.7(4)	753.4(2)	935.3(2)	0.9243	This work
$Yb_2Ir_3Al_9$	1292.7	748.3	936.7	0.9061	[13]
$Lu_2Ir_3Al_9$	1291.4(1)	753.0(1)	935.2(1)	0.9094	This work
$U_2Ir_3Al_9$	1313	758	934	0.930	[10]
$Y_2Pd_3Al_9$	1315.9(1)	766.7(1)	939.9(1)	0.9482	This work
$Gd_2Pd_3Al_9$	1316.6(1)	766.5(1)	943.4(1)	0.9521	This work
$Tb_2Pd_3Al_9$	1315.0(2)	766.4(1)	940.3(1)	0.9477	This work
$Dy_2Pd_3Al_9$	1312.7(2)	764.2(1)	938.0(2)	0.9410	This work
$Ho_2Pd_3Al_9$	1313.7(2)	763.5(1)	935.8(2)	0.9386	This work
$Er_2Pd_3Al_9$	1312.1(2)	762.1(1)	935.2(1)	0.9351	This work
$Tm_2Pd_3Al_9$	1309.9(1)	763.5(1)	934.5(1)	0.9346	This work

[a] Lattice constants of this work were generally determined from samples with the overall composition 2:3:15. For some iridium-containing compounds lattice constants were also determined from samples with the overall composition 1:1:18; those are marked with asterisks.

rare-earth elements were purchased as ingots. Filings of lanthanum and the light lanthanoids were prepared under dry (Na) paraffin oil, which was washed away by dry hexane. Adhering iron particles were removed by a magnet.

Most of the samples were prepared in the atomic ratio R:T:Al = 2:3:15 by arc melting of cold-pressed pellets. Some iridium-containing samples (Table 1) were also synthesized in the atomic ratio 1:1:18 in alumina crucibles, which were sealed in silica tubes under an argon atmosphere (1 bar at 400 K). These samples were heated to 850°C at a rate of 50°C/h, held at that temperature for 500 h, and subsequently cooled to room temperature at a rate of 5°C/h. The excess of aluminum and rare-earth aluminides were dissolved in diluted hydrochloric acid, which attacks the crystals of the ternary compounds at a much slower rate.

All of these ternary aluminides are stable in air and show metallic luster. The energy-dispersive X-ray fluorescence analyses of the crystals in a scanning electron microscope showed no impurities of elements with atomic numbers equal to or greater than sodium.

The samples were characterized by their Guinier powder patterns using Cu$K\alpha_1$ radiation with α-quartz (a = 491.30 pm, c = 540.46 pm) as an internal standard. The lattice constants were refined by least-squares fits. Some of the iridium-containing compounds were isolated from samples with differing overall compositions, resulting in slightly differing lattice constants (Table 1). The plot of the cell volumes (Fig. 1) reflects the expected lanthanoid contraction and indicates mixed or intermediate valence for the cerium and ytterbium

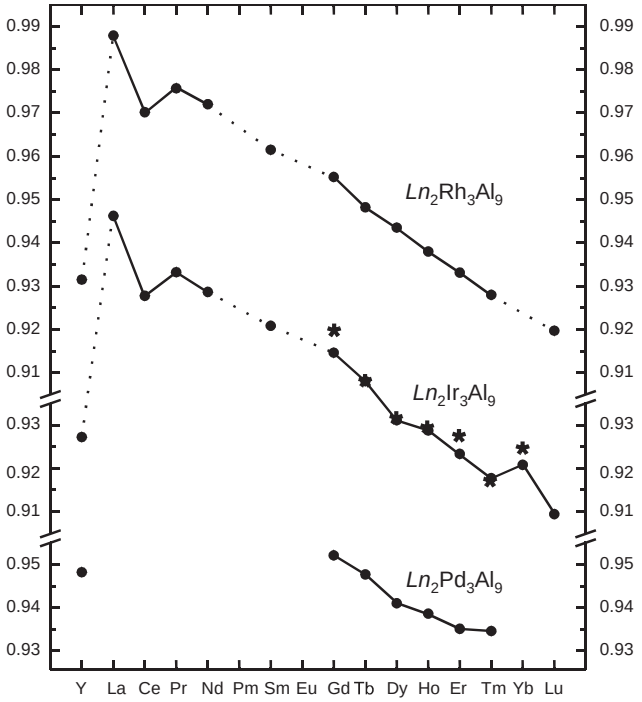

Fig. 1. Cell volumes of aluminides with $Y_2Co_3Ga_9$-type structure. Cell volumes (nm^3) determined from samples with the overall composition 2:3:15 are indicated by filled circles. Cell volumes of certain iridium-containing compounds were determined from samples with the overall composition 1:1:18; these are plotted with asterisks.

compounds, as is well known for many other intermetallics of cerium, europium, and ytterbium.

3. Magnetic properties

The magnetic susceptibilities of the iridium-containing aluminides $R_2Ir_3Al_9$ (R = Y, La–Nd, Sm, Dy–Tm) were determined with a superconducting quantum interference device (SQUID) magnetometer (Quantum Design, Inc.) between 2 and 300 K with magnetic flux densities of up to 5.5 T. Generally, between 10 and 30 mg of each compound were filled into a silica tube (outer diameter 2 mm) and held in place by a cotton plug. The samples were cooled in zero field and the susceptibilities were recorded continuously on heating. To check for ferromagnetic impurities, the field dependence of each sample was determined at 300 K. Only very minor amounts of such impurities were detected. The magnetic properties of all compounds are summarized in Table 2.

The magnetic susceptibilities of $Y_2Ir_3Al_9$ and $La_2Ir_3Al_9$, where the rare-earth elements are not expected to carry magnetic moments, are very small. They show some field dependence indicating some ferromagnetic impurities. However, the susceptibilities at 3 and 5 T were practically the same. Thus, no extrapolation to infinite magnetic flux density was necessary. From the data measured with 3 T we obtained the room-temperature susceptibility values of $1.0(\pm 0.5)\times 10^{-9}\,m^3/mol$ of the formula unit (f.u.) and $2.6(\pm 0.5)\times 10^{-9}\,m^3/f.u.$, respectively. They are almost temperature independent (Fig. 2), indicating Pauli paramagnetism. The upturns of the magnetic susceptibilities at low temperature can be ascribed to minor amounts of paramagnetic impurities or to paramagnetic surface states. The fact that $Y_2Ir_3Al_9$ and $La_2Ir_3Al_9$ do not show any strong magnetic moments shows that the iridium atoms in these compounds are magnetically saturated, and this can also be assumed for the other aluminides of this series.

The magnetic properties of the other rare-earth iridium aluminides $Ln_2Ir_3Al_9$ are dominated by the magnetism of the rare-earth components (Figs. 3–5). The reciprocal susceptibilitiy of the compound $Ce_2Ir_3Al_9$ deviates from the Curie–Weiss law as is frequently observed for cerium compounds, indicating mixed or intermediate valent $Ce^{3+/4+}$. Applying the Curie–Weiss law to the nearly straight portion of this reciprocal susceptibility plot at high temperatures results

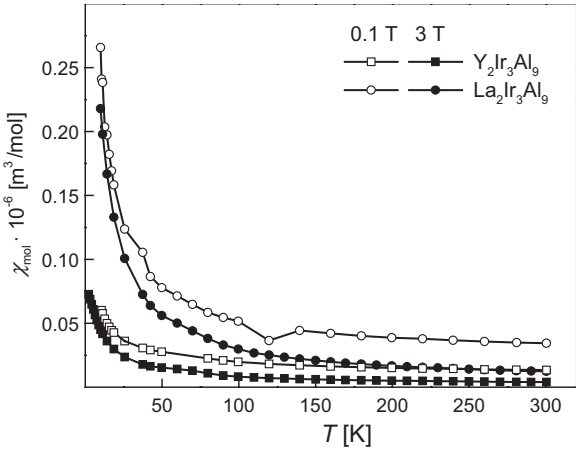

Fig. 2. Temperature dependence of the magnetic susceptibilities of $Y_2Ir_3Al_9$ and $La_2Ir_3Al_9$ recorded with magnetic flux densities of 0.1 and 3 T.

Table 2
Magnetic data for the aluminides $R_2Ir_3Al_9$ (R = Y, La–Nd, Sm, Dy–Tm)[a]

Compound	Magnetic behavior	μ_{exp} (μ_B/R^{3+})	μ_{eff} (μ_B/R^{3+})	Θ (K)	T_N/T_C (K)	$\mu_{sm(exp)}$ (μ_B/R^{3+})	$\mu_{sm(calc)}$ (μ_B/R^{3+})
$Y_2Ir_3Al_9$	Pauli paramagnetic	—	—	—	—	—	—
$La_2Ir_3Al_9$	Pauli paramagnetic	—	—	—	—	—	—
$Ce_2Ir_3Al_9$	Mixed valence	[1.83(2)]	2.54	[–220(5)]	—	0.16(1)	2.14
$Pr_2Ir_3Al_9$	Antiferromagnetic	3.21(2)	3.58	–18(2)	<3	0.47(1)	3.20
$Nd_2Ir_3Al_9$	Antiferromagnetic	3.15(2)	3.62	–18(2)	<3	0.81(1)	3.27
$Sm_2Ir_3Al_9$	Van Vleck behavior	1.46(2)	1.55	—	—	—	—
$Dy_2Ir_3Al_9$	Metamagnetic (?)	10.16(2)	10.65	–10(2)	4(2)	6.10(4)	10
$Ho_2Ir_3Al_9$	Antiferromagnetic (?)	9.97(2)	10.61	–9(2)	4(2)	6.19(4)	10
$Er_2Ir_3Al_9$	Antiferromagnetic (?)	9.28(2)	9.58	–10(2)	3(2)	7.50(4)	9
$Tm_2Ir_3Al_9$	Antiferromagnetic (?)	7.27(2)	7.56	–8(2)	3(2)	5.37(4)	7

[a] The experimentally determined effective magnetic moments μ_{exp} were calculated from the relation $\mu_{exp} = 2.83\times C^{1/2}/(4\pi\times 10^{-6})\,\mu_B$, where the values of C were obtained by fits of the data to the modified Curie–Weiss law $\chi = \chi_0 + C/(T-\Theta)$. They are compared with the theoretical moments μ_{eff}, calculated from the relation $\mu_{eff} = g(J(J+1))^{1/2}\,\mu_B$. The paramagnetic Curie temperatures (Weiss constants) Θ as well as the Néel and Curie temperatures T_N and T_C are listed. The theoretical magnetic moment μ_{eff} for the samarium compound was calculated with the screening constant $\sigma = 33$ with the formula by Van Vleck [18]. The last but one column contains the "saturation" magnetization $\mu_{sm(exp)}$, obtained at 2 K with a magnetic flux density of 5.5 T. These values are compared to the theoretical saturation moments as calculated from the relation $\mu_{sm(calc)} = gJ$. Estimated error limits in the place values of the last listed digits are given in parentheses for all magnetic data of this paper.

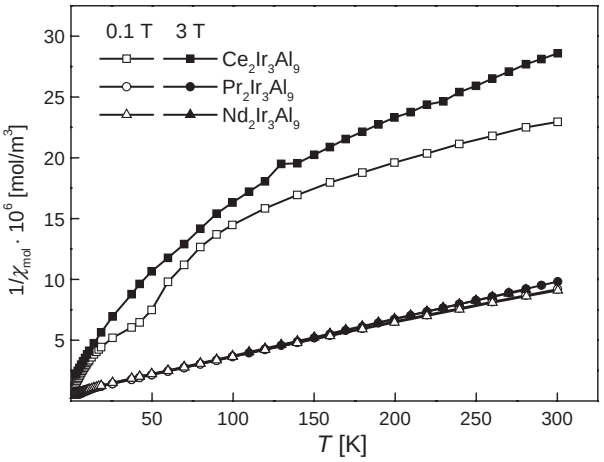

Fig. 3. Reciprocal susceptibilities of the three compounds $Ce_2Ir_3Al_9$, $Pr_2Ir_3Al_9$ and $Nd_2Ir_3Al_9$ as a function of temperature, measured with magnetic flux densities of 0.1 and 3 T. The four curves of $Pr_2Ir_3Al_9$ and $Nd_2Ir_3Al_9$ are practically superimposed.

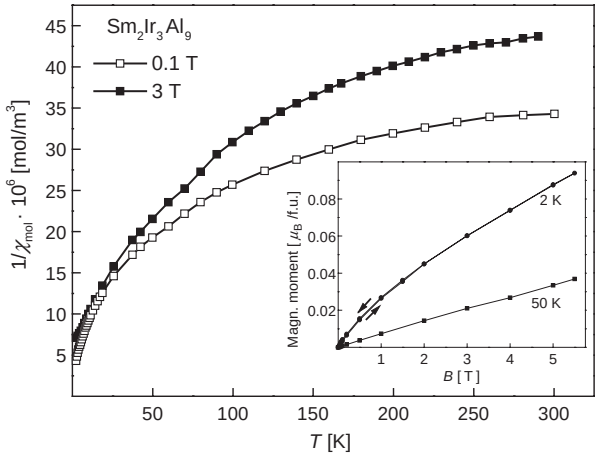

Fig. 4. Magnetic behavior of the samarium compound $Sm_2Ir_3Al_9$. The main diagram shows the temperature dependence of the reciprocal susceptibility, inset is the magnetization measured at 2 and 50 K.

in a magnetic moment of $\mu_{exp} = 1.83(2)\,\mu_B$/Ce, considerably lower than the theoretical moment of $\mu_{eff} = 2.54\,\mu_B/Ce^{3+}$; the corresponding Weiss constant is strongly negative: $\Theta = -220$ K. The reciprocal susceptibility of the cerium compound shows considerable dependence on the magnetic field. This might be ascribed to an (unknown) ferromagnetic impurity. However, since the reciprocal susceptibilities of most other compounds $Ln_2Ir_3Al_9$ investigated by us show considerably less field dependence, it might also be an intrinsic property of the cerium compound. In any case, the Guinier powder pattern of our sample did not show any impurity lines. The reciprocal susceptibility of $Ce_2Ir_3Al_9$ has already been measured earlier [10,11] with the same magnetic flux density of 0.1 T as applied by us. Our data agree rather well with the earlier results at room temperature, but do not show the maximum observed at ca. 50 K. There is agreement in assigning a mixed-valent character to this compound.

The reciprocal susceptibilities of $Pr_2Ir_3Al_9$ and $Nd_2Ir_3Al_9$ show Curie–Weiss behavior with experimental effective moments of $\mu_{exp} = 3.21(2)$ and $3.15(2)$ μ_B/Ln^{3+}, respectively, almost reaching the theoretical effective moments of $\mu_{eff} = 3.58$ and $3.62\ \mu_B/Ln^{3+}$. The difference might be ascribed to crystal field effects. The Weiss constants Θ are negative (Table 2) suggesting antiferromagnetic order at low temperatures. The magnetization curves for these two compounds (not shown) recorded at 2 K show linear field dependence without any hystereses, reaching at 5.5 T approximately 15% and 25%, respectively, of the theoretical saturation moments $\mu_{sm(calc)}$ of 3.20 and 3.27 μ_B/Ln^{3+}.

The temperature dependence of the reciprocal susceptibility of $Sm_2Ir_3Al_9$ is plotted in Fig. 4. It shows a behavior which is typical for Sm^{3+} compounds as described by Van Vleck. A magnetic moment of $\mu_{exp} = 1.46(2)\ \mu_B/Sm^{3+}$ was calculated from the magnetic susceptibility measured at $T = 300$ K with a flux density of 3 T using the equation $\mu_{exp} = 2.83(T\chi/2)^{1/2}(4\pi \times 10^{-6})^{1/2}\,\mu_B$. This value compares reasonably well with the theoretical value of $\mu_{eff} = 1.55\,\mu_B$ calculated by the Van Vleck formula with the screening constant $\sigma = 33$ [18].

All of the other iridium-containing aluminides show Curie–Weiss behavior above 50 K (Fig. 5). The reciprocal susceptibilities of these compounds $Ln_2Ir_3Al_9$ (Ln = Dy–Tm) were all slightly dependent on the applied magnetic field, indicating ferromagnetic impurities. However, in all cases we obtained practically the same susceptibility values at 3 and 5 T. Thus, we did not extrapolate to infinite magnetic flux densities and extracted our reciprocal susceptibility results from the data recorded at 3 T. As can be seen from the results summarized in Table 2, the effective magnetic moments μ_{exp}, calculated from the straight portions of the $1/\chi$ vs. T plots above 100 K, are all in reasonable agreement with the theoretical effective magnetic moments μ_{eff}, calculated for the free Ln^{3+} ions from the relation $\mu_{eff} = g[J(J+1)]^{1/2}\,\mu_B$, where g is the Landé factor and J is the total angular momentum number. The small differences between the experimental and the theoretical effective moments μ_{exp} and μ_{eff} can again be ascribed to crystal field effects. The Weiss constants Θ of these compounds are all slightly negative, varying between $-8(2)$ and $-10(2)$ K, indicating antiferromagnetic coupling of the magnetic moments. The magnetic ordering temperatures of the compounds $Ln_2Ir_3Al_9$ (Ln = Dy–Tm) are all low, at temperatures of 4 K or lower. Thus, the magnetization curves of these four compounds, measured at 2 K (insets of Fig. 5), do not allow to draw any firm conclusions about the magnetic order below the ordering temperatures. Metamagnetism seems to be indicated for the dysprosium compound. No saturation

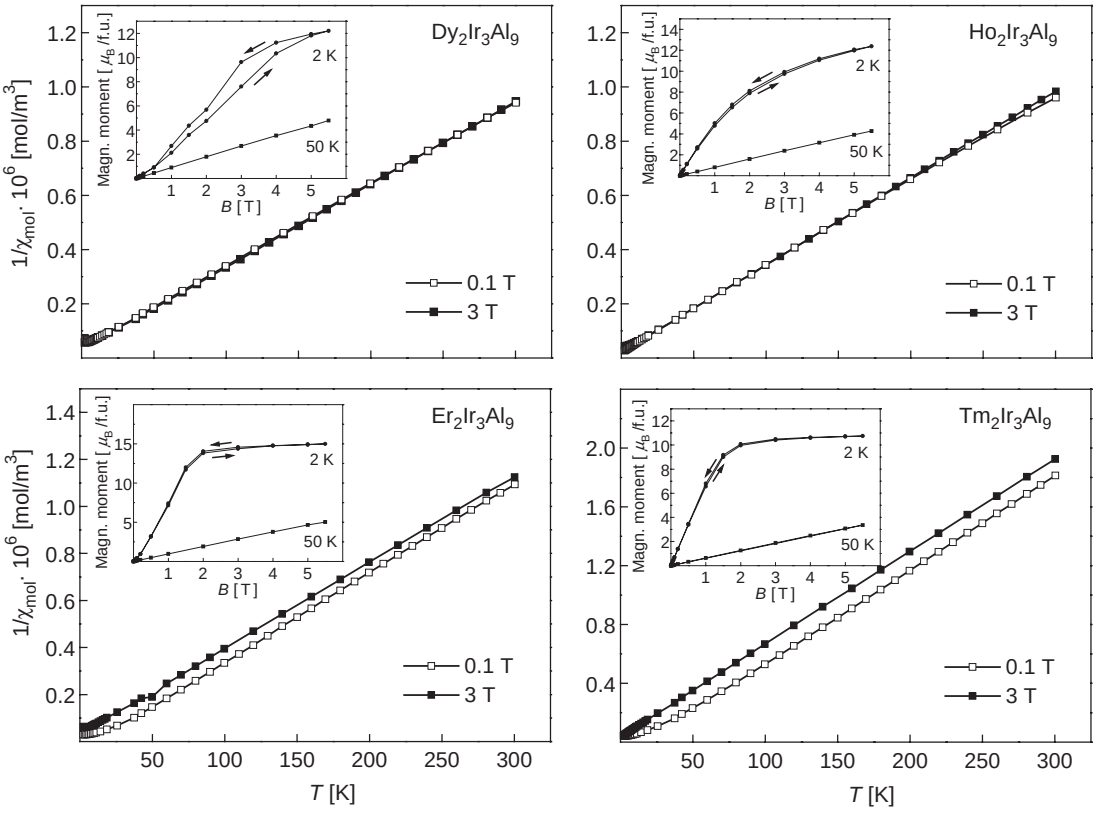

Fig. 5. Magnetic properties of the four rare-earth iridium aluminides $Ln_2Ir_3Al_9$ (Ln = Dy–Tm). The main plots show the temperature dependence of the reciprocal susceptibilities $1/\chi$ measured in magnetic fields of 0.1 and 3 T. The insets show the magnetization as a function of the magnetic flux density B recorded at temperatures of 2 and 50 K.

is reached at 5.5 T (the highest magnetic flux density obtainable with our SQUID magnetometer) for $Dy_2Ir_3Al_9$ and $Ho_2Ir_3Al_9$. The experimentally obtained magnetizations $\mu_{sm(exp)}$ at this magnetic field strength for our samples of $Er_2Ir_3Al_9$ and $Tm_2Ir_3Al_9$ amount to ca. 80% of the theoretical values $\mu_{sm(calc)}$ (Fig. 5, Table 2).

4. Structure refinements

Single crystals of $Ho_2Rh_3Al_9$ and $Er_2Ir_3Al_9$ were isolated from crushed samples. They were investigated with a Buerger precession camera to establish their suitability for the intensity data collection. These data were measured using an Enraf Nonius CAD4 diffractometer with graphite-monochromated Mo$K\alpha$ radiation and a scintillation counter with pulse-height discrimination. The scans were along the Laue streaks ($\theta/2\theta$) with background counts at both ends of each scan. Absorption corrections were applied from psi scan data. Further details of the data collection and some results of the structure refinements are summarized in Table 3.

The structures were refined with a full-matrix least-squares program of the program package SHELX-97 [19] using atomic scattering factors, corrected for anomalous dispersion as provided by the program. The weighting schemes accounted for the counting statistics and a parameter correcting for secondary extinction was optimized as a least-squares variable.

It must be mentioned that both structure determinations and refinements were not straightforward. For both single crystals, the software of the four-circle diffractometer found a small hexagonal cell which turned out to correspond to a subcell of the real structure. The hexagonal subcell is indicated with dashed lines in the atomic layers of the structure shown at the right-hand side of Fig. 6. The orthorhombic cell dimensions a_o, b_o, and c_o are related to the hexagonal subcell with the translation periods a_h and c_h as follows: $a_o = 3a_h$, $b_o = a_h\sqrt{3}$, and $c_o = c_h$. The corresponding hexagonal structure belongs to the space group $P6_3mc$ (No. 186), has only five atomic positions, only seven variable positional parameters, and could be refined for $Er_2Ir_3Al_9$ to a conventional residual of $R(F) = 0.011$ with reasonable thermal parameters. The only drawback is that not all atomic positions are fully occupied and that there are some too short interatomic distances. An ordered model for the structure was then postulated with a larger C centered orthorhombic cell. Subsequently, the corresponding superstructure reflections were found also on the four-circle diffractometer, and the intensity data were again collected for this six times

Table 3
Single-crystal data of $Ho_2Rh_3Al_9$ and $Er_2Ir_3Al_9$

Ideal composition	$Ho_2Rh_3Al_9$	$Er_2Ir_3Al_9$
Sample composition	2:3:15	1:1:18
Space group	*Cmcm* (No. 63)	*Cmcm* (No. 63)
Lattice constants		
a (pm)	1316.8(3)	1313.8(2)
b (pm)	760.2(2)	758.5(1)
c (pm)	933.7(2)	933.8(2)
V (nm^3)	0.9346	0.9305
Formula units/cell, *Z*	*Z* = 4	*Z* = 4
Formula mass	881.41	1154.01
Calculated density, ρ (g/cm^3)	6.26	8.24
Crystal size (μm)	$33 \times 22 \times 44$	$22 \times 22 \times 44$
Scans up to 2θ (deg)	66	70
Range in *h k l*	$\pm 18, \pm 11, \pm 14$	$\pm 21, \pm 11, 0$–13
Total number of reflections	3982	2943
Unique reflections	822	775
Internal residual, R_i (all F_o^2)	0.117	0.033
Reflections with $F_o > 2\sigma(F_o)$	255	392
Highest/lowest transmission	1.14	1.07
Number of variables	27	27
Conventional residual, $R(F > 2\sigma)$	0.044	0.057
Weighted residual, R_w (all F^2)	0.084	0.109
Highest/lowest residual electron density ($e/Å^3$)	5.0/−5.9	4.4/−6.5

larger cell for both compounds. The orthorhombic distortion of the hexagonal subcell manifests itself also in the Guinier powder diagrams. It results in a splitting of the strong subcell reflections, which is clearly visible, especially for reflections at high 2θ values. In addition, on close inspection, the rather weak superstructure reflections corresponding to the larger orthorhombic cell were observed in almost all powder diagrams.

For the orthorhombic cell the computer software evaluating the single-crystal data [20] suggested the space group *Cmcm* (No. 63). The positions of the heavy atoms were then located by the Patterson method and the other positions by difference Fourier syntheses. Eventually the structure was recognized to essentially be isotypic with that of $Y_2Co_3Ga_9$ [7]. However, if only atomic positions corresponding to those of $Y_2Co_3Ga_9$ were refined, the difference Fourier syntheses revealed residual electron densities which were recognized to be due to misplaced atomic layers of the type *A* shown in Fig. 6. For each correctly positioned atomic layer *A*, there are two additional possibilities for misplaced atomic layers of the same type, as is shown at the lower left-hand side of Fig. 6. It can be seen, that the main (correctly placed) layer and the two additional (misplaced) layers differ by one- and two-thirds, respectively, of the translation period *a*. We then thought of how to include the misplaced layers in the least-squares refinements. In principle, these two misplaced layers do not need to occur in equal amounts. However, if the refinement is to be carried out in the space group *Cmcm* they necessarily obtain equal occupancies. We then calculated the atomic positions for the two symmetry-related misplaced layers and refined constrained occupancies for the main and the misplaced layers together with the atomic parameters of main layer *A* and layer *B*. Subsequently, the positional parameters of the misplaced layers were again adjusted to the just obtained positional parameters of the main layers. The final occupancy parameters of the main layer and the misplaced layers were found by iteration, looking for a minimum in the weighted residuals R_w. For the structure of $Ho_2Rh_3Al_9$ we obtained an occupancy of 66.5(1)% for the main layer; for the structure of $Er_2Ir_3Al_9$ the corresponding value is 73.0(1)%. The misplaced layers are designated with the atomic symbols Ho(a)/Er(a), Al(3a), Al(3b), and Al(4a) in Table 4. The highest residual electron densities in the final difference Fourier syntheses amounted to the relatively low values of 5.0 and $4.4\,e/Å^3$ for the structures of $Ho_2Rh_3Al_9$ and $Er_2Ir_3Al_9$, respecvtively, thus indicating that the misplaced layers were essentially correctly positioned in the final refinements. The atomic parameters of the misplaced layers are listed without standard deviations in Table 4, since they were not varied independently of the main layers.

5. Discussion

We have prepared 29 new rare-earth rhodium, iridium, or palladium-containing aluminides with $Y_2Co_3Ga_9$-type structure. Altogether there are now some 90 compounds with this structure type, including the aluminides listed above, which in addition to platinum metals, may also contain cobalt as transition metal component [8–13]. Corresponding gallium compounds $R_2T_3Ga_9$ are known with *T* = Co [7], Rh [21], and Ir [21] as well as with ruthenium as transition metal [22]. The lattice constants of the new aluminides are listed in Table 1. We have isolated several of the iridium-containing compounds from samples with differing overall compositions (*R*:Ir:Al = 2:3:15 or 1:1:18). On careful inspections, the corresponding Guinier powder patterns showed noticeable differences. The evaluation of these patterns resulted in systematic differences of up to 0.5% for the lattice constants of corresponding compositions. Thus, these compounds show homogeneity ranges.

The $Y_2Co_3Ga_9$-type structure has been discussed as being built up of two kinds of slabs cut from the CsCl- and Th_3Pd_5-type structures [8]. Recently, it became more appropriate to describe this structure as consisting of two kinds of layers which we have emphasized in Fig. 6 with $Ho_2Rh_3Al_9$ as example. The layers of the type *A* contain the holmium atoms and additional aluminum atoms in the ratio Ho:Al = 2:3. These layers

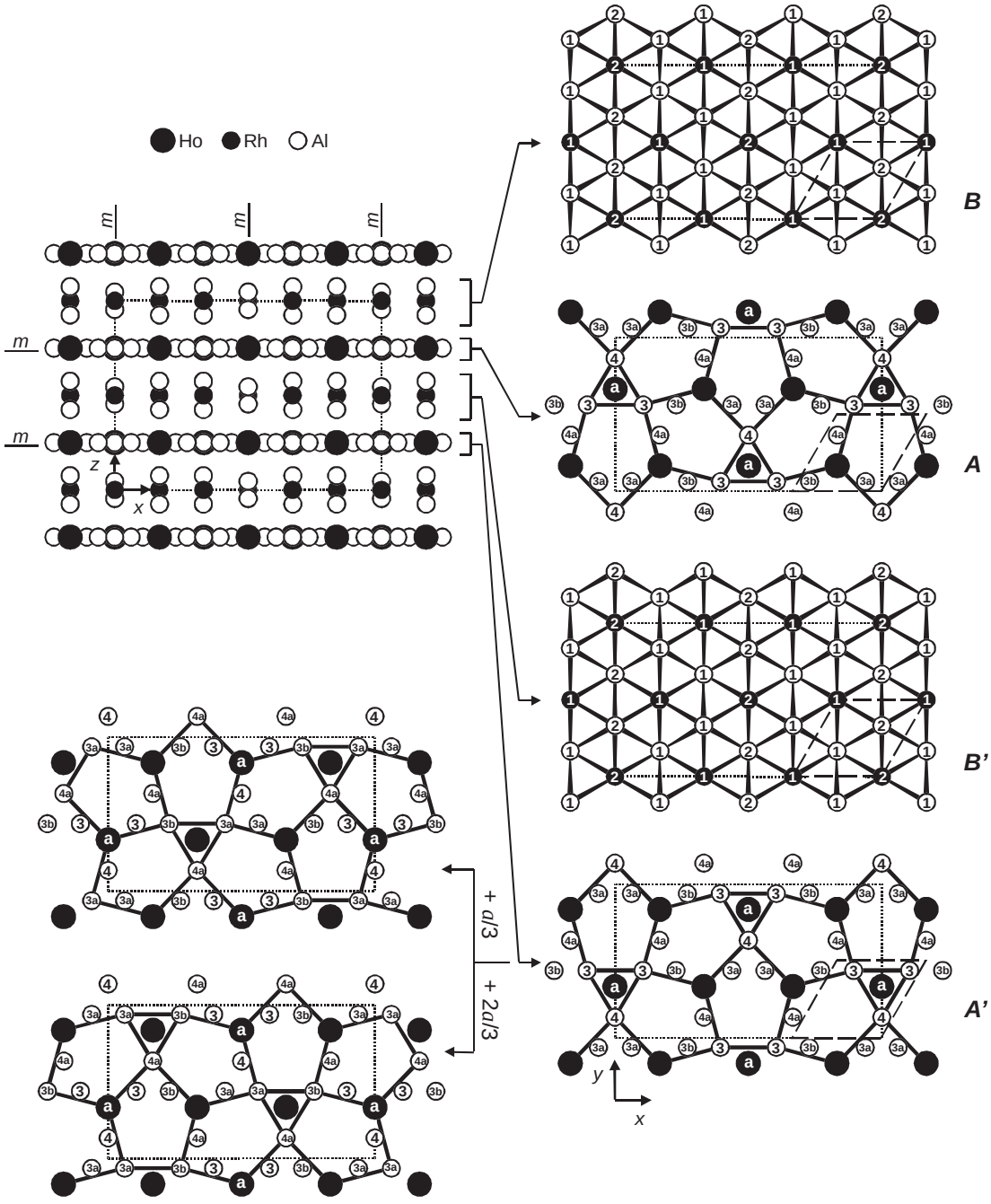

Fig. 6. The crystal structure of $Ho_2Rh_3Al_9$. In the upper left-hand corner the whole structure is projected along the y-axis. Four atomic layers of this projection are shown at the right-hand side in projections along the z-axis. All atomic positions as found during the structure refinements are shown. In the layers of type A, atomic positions found with an occupancy of 66.5%, are connected by lines in the right-hand side of the figure. In the lower left-hand part, the other atomic positions are connected. They belong to two misplaced A layers and are found—because of the space group symmetry—with the same occupancy of 16.75%. Single-digit numbers and letters "a" and "b" correspond to the atom designations. In the layers shown at the right-hand side, the small hexagonal subcell discussed in the text is indicated with dashed lines.

correspond to mirror planes and consequently they are perfectly planar. The layers of the type B consist of rhodium atoms and aluminum atoms in the ratio Rh:Al = 1:2. These layers are hexagonal close packed, however not planar, but slightly puckered. The puckering is such that the positions of the six aluminum atoms surrounding a rhodium atom within one layer B correspond to those of a very compressed octahedron. In the perfect $Y_2Co_3Ga_9$-type structure these layers alternate in the sequence $ABA'B'$, $ABA'B'$ [2,22,23]. Layers B and B' look very similar when viewed along the stacking direction; however, they differ in the kind of

Table 4
Atom parameters of $Ho_2Rh_3Al_9$ and $Er_2Ir_3Al_9$[a]

Atom	*Cmcm*	Occupancy	*x*	*y*	*z*	*B*
$Ho_2Rh_3Al_9$						
Ho	8*g*	0.665(1)	0.3331(3)	0.3336(1)	1/4	0.81(1)
Rh(1)	8*e*	1	0.3332(4)	0	0	0.23(1)
Rh(2)	4*a*	1	0	0	0	0.27(3)
Al(1)	16*h*	1	0.1677(9)	0.1663(3)	0.0754(2)	0.31(2)
Al(2)	8*f*	1	0	0.3324(7)	0.5461(4)	0.31
Al(3)	8*g*	0.665	0.1049(6)	0.437(1)	1/4	1.36(7)
Al(4)	4*c*	0.665	0	0.134(1)	1/4	1.36
Ho(a)	4*c*	0.670	0	0.3336	1/4	0.81
Al(3a)	8*g*	0.1675	0.4382	0.437	1/4	1.36
Al(3b)	8*g*	0.1675	0.2284	0.437	1/4	1.36
Al(4a)	8*g*	0.1675	0.3333	0.134	1/4	1.36
$Er_2Ir_3Al_9$						
Er	8*g*	0.730(1)	0.3342(1)	0.3336(1)	1/4	1.02(1)
Ir(1)	8*e*	1	0.3317(1)	0	0	0.41(1)
Ir(2)	4*a*	1	0	0	0	0.53(1)
Al(1)	16*h*	1	0.1669(3)	0.1652(4)	0.0714(3)	0.70(3)
Al(2)	8*f*	1	0	0.3305(8)	0.5526(5)	0.70
Al(3)	8*g*	0.730	0.1023(6)	0.439(1)	1/4	1.9(1)
Al(4)	4*c*	0.730	0	0.123(1)	1/4	1.9
Er(a)	4*c*	0.540	0	0.3336	1/4	1.02
Al(3a)	8*g*	0.135	0.4356	0.439	1/4	1.9
Al(3b)	8*g*	0.135	0.2310	0.439	1/4	1.9
Al(4a)	8*g*	0.135	0.3333	0.123	1/4	1.9

[a] Both structures contain misplaced atomic layers consisting of the atoms Ho(a), Er(a), Al(3a), Al(3b), and Al(4a). Concerning the refinement of the atomic parameters of these misplaced layers see text. The last column contains the isotropic displacement parameters ($\times 10^4$ pm^2) of the aluminum atoms and the equivalent isotropic displacement parameters of the other atoms. Parameters listed without standard deviations were refined constrained to corresponding parameters listed with standard deviations.

puckering. A layers *A* between a layer *B* and a layer *B′* corresponds to a mirror plane. Thus, the puckered layers *B* and *B′* are mirror images of each other. The difference between layers *A* and *A′* is readily recognized when the orientations of the small triangles, formed by one Al(4) and two adjacent Al(3) atoms, is considered. In layer *A* (shown on the right-hand side of Fig. 6), the Al(4) atoms of such a triangle point upwards while they point downwards in layer *A′*.

Our structure refinements of $Ho_2Rh_3Al_9$ and $Er_2Ir_3Al_9$ showed that 33.5(1)% and 27.0(1)%, respectively, of the *A* layers in their $Y_2Co_3Ga_9$-type structure are misplaced. These misplaced layers seem to substitute for regularly placed layers in a more or less irregular way. At least we have not observed any superstructure reflections which would result if layers *A* would have long-range order with a more complicated stacking sequence. Nevertheless, it seems possible that corresponding more complicated structures may still be discovered in samples annealed for long time at relatively low temperatures. However, the corresponding superstructure reflections would be rather weak, because they would result from the order of only a small fraction of the total scattering power.

In the lower right-hand part of Fig. 6, we have outlined a small hexagonal subcell for layer *A′*. This subcell contains three aluminum atoms—Al(3), Al(3), and Al(4)—which may be substituted by a holmium atom—Ho(a). Actually, during the structure refinements of $Ho_2Rh_3Al_9$ and $Er_2Ir_3Al_9$ we have considered such random substitutions to account for the disorder found in the layers of the type *A* and *A′*. It was possible to refine our single-crystal data with such a substitution model, in contrast to the shift model finally considered to be correct. This substitution model resulted in the compositions $Ho_{1.83(1)}Rh_3Al_{9.65(2)}$ and $Er_{1.78(1)}Ir_3Al_{9.59(3)}$ with relatively low residuals of $R = 0.022$ (233 *F* values, 49 variables) and $R = 0.029$ (411 *F* values, 51 variables), respectively. However, for steric reasons this substitution model cannot possibly be correct, because the substitution of a rare-earth atom by three aluminum atoms results in too short Al–Al distances for aluminum atoms belonging to neighboring subcells. In contrast, the inverse substitution (three aluminum atoms of a subcell are replaced by a rare-earth atom) is sterically possible.

The structure of $Er_4Pt_9Al_{24}$ has been described as a stacking variant of $Y_2Co_3Ga_9$ [2]. The composition of the two compounds differs, because in the structure of the erbium compound two layers of the type *B* are adjacent to each other, corresponding to the stacking sequence *ABBAB*, *ABBAB*. Other structures

of intermetallics with a high content of aluminum or gallium consisting of various stackings of layers of the type *A* (containing a loose arrangement of the rare-earth atoms with aluminum or gallium atoms) and *B* (containing the transition metal atoms with aluminum or gallium in hexagonal close packed arrangement) are $LuRe_2Al_{10}$ and $YbFe_2Al_{10}$ [24], $TbRe_2Al_{10}$ [23], $CeOsGa_4$ [25], $Gd_3Ru_4Al_{12}$ [3,26], $Ho_3Ru_4Ga_{15}$ [27], $Sc_{1.2}Fe_4Si_{9.8}$ [4,28], and $Y_{7.28}Re_{12}Al_{61.38}$ [5,29]. In this context we must emphasize that for topological reasons the description of these structures as consisting of layers is very convenient and convincing. However, one has to be aware that the mechanical properties of these compounds do not reflect the layered topology. For example, it is well known that the layers in graphite or in various transition metal disulfides (e.g., MoS_2) can easily be shifted relative to each other by directional external pressure. In contrast, in the structures of the aluminides and gallides enumerated above, chemical bonding within and between the layers is of similar strength. Thus, grinding of the samples in a mortar results in grains of approximately uniform dimensions.

Table 5 lists the interatomic distances between the atomic positions with high populations (disregarding atomic positions of misplaced layers of the type *A*) for the structures of $Ho_2Rh_3Al_9$ and $Er_2Ir_3Al_9$. It can be expected that the corresponding distances are of similar lengths in the two structures, since the metallic radii [30,31] for the corresponding atoms are very similar: holmium ($r = 176.6$ pm) is slightly larger than erbium (175.7 pm), and rhodium (134.5 pm) is slightly smaller than iridium (135.7 pm). The differences between corresponding interatomic distances are much larger than those of the lattice constants. The latter differ by 1% or less. In contrast, the interatomic distances in the two compounds differ by up to 3.0% (10σ) in both directions. For instance the (only very weakly bonding) Al(1)–Al(1) distance of 326.2 pm in $Ho_2Rh_3Al_9$ is considerably smaller than the corresponding distance of 333.6 pm in $Er_2Ir_3Al_9$. In contrast, the Ho–Al(4) distance of 317.0 pm is considerably larger than the Er–Al(4) distance of 309.3 pm. Nevertheless, these largest differences are possibly partially due to unfortunate combinations of errors.

The $Y_2Co_3Ga_9$-type structure and its near-neighbor coordinations have been described and discussed earlier for the prototype [7] as well as for the isotypic aluminide $Y_2Co_3Al_9$ [8]. The near-neighbor environments have been discussed recently also for $Dy_2Ru_3Ga_9$ [22], and—as could be expected—those of the aliminides are very similar to those of the gallides. The rare-earth atoms of this structure are well separated from each other with the shortest distances Ho–Ho and Er–Er, of the aluminides presented here, amounting to 439 and 435 pm, respectively. Since the transition metal atoms do not carry magnetic moments, the magnetic order is

Table 5
Interatomic distances in $Ho_2Rh_3Al_9$ and $Er_2Ir_3Al_9$[a]

Ho/Er	2Al(1)	300.0/304.0
	2Al(1)	300.8/301.8
	2Al(1)	303.8/300.1
	1Al(3)	310.5/315.0
	1Al(3)	312.7/310.7
	2Al(2)	317.0/311.4
	1Al(4)	317.0/309.3
	2Rh/Ir(1)	344.1/343.4
	2Rh/Ir(2)	344.7/343.3
	2Rh/Ir(1)	344.7/344.3
Rh/Ir(1)	2Al(3)	251.9/253.3
	2Al(2)	257.5/260.5
	2Al(1)	261.1/258.8
	2Al(1)	263.3/262.5
	2Ho/Er	344.1/343.4
	2Ho/Er	344.7/344.3
Rh/Ir(2)	2Al(4)	254.7/251.5
	2Al(2)	256.5/255.3
	4Al(1)	264.4/261.2
	4Ho/Er	344.7/343.3
Al(1)	1Rh/Ir(1)	261.1/258.8
	1Rh/Ir(1)	263.3/262.5
	1Rh/Ir(2)	264.4/261.2
	1Al(3)	275.3/279.6
	1Al(4)	276.0/277.3
	1Al(2)	279.0/277.7
	1Al(1)	287.4/286.4
	1Al(1)	289.2/283.9
	1Ho/Er	300.0/304.0
	1Ho/Er	300.8/301.8
	1Ho/Er	303.8/300.1
	1Al(1)	326.2/333.6
Al(2)	1Rh/Ir(2)	256.6/255.3
	2Rh/Ir(1)	257.5/260.5
	1Al(2)	268.8/275.4
	2Al(1)	279.0/277.7
	2Al(3)	293.4/287.6
	1Al(4)	315.0/323.7
	2Ho/Er	317.0/311.4
	2Al(3)	319.1/323.4
Al(3)	2Rh/Ir(1)	251.9/253.3
	1Al(4)	268.2/274.7
	2Al(1)	275.3/279.6
	1Al(3)	276.2/268.8
	2Al(2)	293.4/287.6
	1Ho/Er	310.5/315.0
	1Ho/Er	312.7/310.7
	2Al(2)	319.1/323.5
Al(4)	2Rh/Ir(2)	254.7/251.5
	2Al(3)	268.2/274.7
	4Al(1)	276.0/277.3
	2Al(2)	315.0/323.2
	2Ho/Er	317.0/309.4

[a] These distances were calculated with the lattice constants as determined from the single-crystal data. The standard deviations are all equal to or smaller than 0.9 pm. All distances smaller than 420 pm (Ho/Er–Ho/Er, Ho/Er–Rh/Ir, Ho/Er–Al, Rh/Ir–Rh/Ir, Rh/Ir–Al) and 370 pm (Al–Al), respectively, are listed. Only distances between atomic sites belonging to atomic layers with high populations are listed. Interatomic distances for the sites Ho(a), Er(a), Al(3a), Al(3b), and Al(4a) are similar to those of the corresponding atoms in the main layers.

likely to be established via the conduction electrons (RKKY theory). The large separation of the rare-earth atoms correlates with the low magnetic ordering temperatures of these compounds.

Acknowledgments

The authors thank Dipl-Ing. U.Ch. Rodewald for the competent collection of the single-crystal data. Dr. W. Gerhartz (Degussa) and Dr. G. Höfer (Heraeus Quarzschmelze, Hanau) supported this work by generous gifts of platinum metals and silica tubes, respectively. We also acknowledge the support of the Deutsche Forschungsgemeinschaft, the Fonds der Chemischen Industrie, and the International Center for Diffraction Data.

References

[1] V.M.Th. Thiede, Th. Ebel, W. Jeitschko, J. Mater. Chem. 8 (1998) 125.
[2] V.M.Th. Thiede, B. Fehrmann, W. Jeitschko, Z. Anorg. Allg. Chem. 625 (1999) 1417.
[3] J. Niermann, W. Jeitschko, Z. Anorg. Allg. Chem. 628 (2002) 2549.
[4] J. Niermann, W. Jeitschko, Z. Anorg. Allg. Chem. 630 (2004) 361.
[5] J. Niermann, W. Jeitschko, Inorg. Chem., accepted for publication.
[6] B. Fehrmann, W. Jeitschko, J. Alloys Compd. 298 (2000) 153.
[7] Yu.N. Grin', R.E. Gladyshevskii, O.M. Sichevich, V.E. Zavodnik, Ya.P. Yarmolyuk, I.V. Rozhdestvenskaya, Sov. Phys. Crystallogr. 29 (1984) 528.
[8] R.E. Gladyshevskii, K. Cenzual, E. Parthé, J. Alloys Compd. 182 (1992) 165.
[9] R.E. Gladyshevskii, K. Cenzual, E. Parthé, Z. Kristallogr. 203 (1993) 113.
[10] B. Buschinger, C. Geibel, M. Weiden, C. Dietrich, G. Cordier, G. Olesch, J. Köhler, F. Steglich, J. Alloys Compd. 260 (1997) 44.
[11] B. Buschinger, O. Trovarelli, M. Weiden, C. Geibel, F. Steglich, J. Alloys Compd. 275–277 (1998) 633.
[12] A. Hiess, S. Coad, B. Buschinger, O. Trovarelli, J.X. Boucherle, F. Givord, T. Hansen, E. Lelievre-Berna, E. Suard, C. Geibel, F. Steglich, Physica B 259–261 (1999) 343.
[13] O. Trovarelli, C. Geibel, B. Buschinger, R. Borth, S. Mederle, M. Grosche, G. Sparn, F. Steglich, O. Brosch, L. Donnevert, Phys. Rev. B 60 (1999) 1136.
[14] A.G. Jackson, Y.R. Mahajan, S.D. Kirchoff, Scr. Metall. 20 (1986) 1247.
[15] J.F. Nie, S. Sridha, B.C. Muddle, Metall. Trans. 23A (1992) 3193.
[16] P. Li, S. Dai, Ch. Li, Mater. Sci. Eng. A 280 (2000) 128.
[17] J. Niermann, B. Fehrmann, W. Jeitschko, Z. Kristallogr. Suppl. 18 (2001) 146.
[18] J.H. Van Vleck, The Theory of Electric and Magnetic Susceptibilities, Oxford University Press, London, 1932.
[19] G.M. Sheldrick, SHELX-97, Program for Crystal Structure Determination, Universität Göttingen, Germany, 1997.
[20] SHELXTL PLUS Release 4.21/V, Siemens Analytical Instruments Inc., Madison, WI, USA, 1990.
[21] Yu.N. Grin, P. Rogl, Izv. Akad. Nauk SSSR, Neorg. Mater. 25 (1989) 593.
[22] M. Schlüter, W. Jeitschko, Z. Anorg. Allg. Chem. 626 (2000) 2217.
[23] B. Fehrmann, W. Jeitschko, Z. Naturforsch. 54b (1999) 1277.
[24] B. Fehrmann, W. Jeitschko, Inorg. Chem. 38 (1999) 3344.
[25] M. Schlüter, W. Jeitschko, Z. Anorg. Allg. Chem. 628 (2002) 1505.
[26] R.E. Gladyshevskii, O.R. Strusievicz, K. Cenzual, E. Parthé, Acta Crystallogr. B 49 (1993) 474.
[27] M. Schlüter, W. Jeitschko, J. Solid State Chem. 172 (2003) 27.
[28] B.Ya. Kotur, M. Bruvo, Sov. Phys. Crystallogr. 36 (1991) 787.
[29] S. Niemann, W. Jeitschko, J. Alloys Compd. 221 (1995) 235.
[30] E. Teatum, K. Gschneidner, J. Waber, LA-2345, US Department of Commerce, Washington, DC, 1960.
[31] W.B. Pearson, The Crystal Chemistry and Physics of Metals and Alloys, Wiley, New York, 1972.